Topological Order and Degenerate Entanglement Spectrum in Two-Dimensional Dimerized Quantum Heisenberg Model

Ching-Yu Huang* and Feng-Li Lin†

Department of Physics, National Taiwan Normal University, Taipei, 116, Taiwan

Abstract

We study the connection between topological order and degeneracy of the entanglement spectrum by explicitly solving the two-dimensional dimerized quantum Heisenberg model in the form of tensor product state ansatz. By evaluating the topological entanglement entropy, we identify a new phase with topological order in this model, in which the entanglement spectrum is doubly degenerate. Degeneracy of the entanglement spectrum is robust against various types of perturbations, in accordance with our expectation for topological order. Our results support the connection among topological order, long range entanglement and the dominant degenerate singular values of entanglement spectrum. In the context of tensor product state ansatz, the numerical evaluation of entanglement spectrum costs far less computation power than the one for topological entanglement entropy. Our results provide a more viable way to numerically identify the topological order for the generic frustrated systems.

* 896410093@ntnu.edu.tw

† linfengli@phy.ntnu.edu.tw

I. INTRODUCTION

Investigation of topological orders for spin models is under intensive study in the recent years, partly due to its relation to the ground state of high Tc superconductor, the so called spin liquid phase [1], and partly because of the enlightenment of quantum information to characterize the ground states by quantum entanglement [2]. These studies lead to new classification schemes [3–7] of the quantum phases beyond the usual Landau-Ginzburg-Wilson paradigm. The new quantum phases such as the spin liquids are called the topological phases and cannot be characterized by a local order parameter. Instead, it could be characterized by the ground state degeneracy, quasiparticle statistics, existence of edge states, topological entanglement entropy [12, 13], and entanglement spectrum [14]. The latter twos are motivated by the quantum information on the entangled nature of ground state [9]. One typical example for all the above characteristics of topological ordered state is the fractional quantum Hall states [14–16].

For one-dimensional (1D) spin chain the quantum fluctuation could be more significant than in the higher dimensions to melt the system into liquid, and thus becoming topological. The simplest example of the "topological phase" is the Haldane phase. The term with the quotation remark is to mean that the topological nature of the ground state is protected by some symmetry of the spin chain [6, 7]. Once the symmetry is broken, the ground state wave function is equivalent to the trivial product state up to some local unitary transformation [32] by removing the short range entanglement (SRE), i.e., entanglement between the neighboring sites. In contrast, the long range entanglement (LRE) is the entanglement among the distant sites, and causes the topological order of the nontrivial ground state, which is not equivalent to the product state by the local unitary transformation.

On the other hand, for two-dimensional (2D) spin systems the topological phase is usually expected to exist in the frustrated systems since the large ground state degeneracy of the system is highly quantum and cannot have simple classical order. However, suffering from the lack of the reliable numerical tools in solving the 2D frustrated spin systems, only very few topological phases have been identified, such as the toric code model [10, 11]. The

connection between the topological order and the quantum entanglement is less understood than in the 1D cases.

Despite of the recent progress in [3–7] on the general scheme of classifying the topological orders caused by the LRE, it is still not easy in practical to dynamically determine if exists a topological phase. It is then desirable to find a more numerical viable characterization for the topological order. Since the topological order is believed to be linked to the LRE, we think the degeneracy pattern of the entanglement spectrum can be such an index. The intuitive picture is that the entanglement spectrum is the singular (Schmidt) values of the bi-partition of the whole system [7, 8], so the dominant degenerate singular values implies that the wave function is close to the maximally entangled state (GHZ state). In this case, the two parts of the system is coherently long-range entangled.

Moreover, the entanglement spectrum is very easy to evaluate numerically in the ansatz of matrix product states (MPS) or tensor product states (TPS). Indeed, the connection between entanglement spectrum and topological order is established for the MPS numerically [7], however, for the TPS in 2D system it is not clear.

The main motivation of this paper is to establish such an connection in 2D among topological order, long range entanglement and degenerate entanglement spectrum by numerically studying a particular frustrated 2D spin model with its ground state in the form of the TPS ansatz. In the meantime we explore the properties of the entanglement spectrum under various types of the local unitary transformations to test its robustness, which is also the characteristics of the topological order.

The model we will study is the staggered dimer spin 1/2 model on the square lattice, and will be referred as the J-J' model form now on. It is an interesting 2D spin model with various issues about quantum phase transition. For the antiferromagnetic J'-bond regime, i.e., $J'/J > 0$, this model has been studied by using the perturbation theory [17], exact diagonalization (ED) [19], the coupled cluster method (CCM) [19], iPEPS [20] and quantum Monte Carlo [21, 22]. In this regime, there exists a quantum phase transition by tuning J' with a critical point at $J'/J \approx 2.51$ [17], separating the classical Néel ordered phase and a finite-gap disordered phase [21, 22].

In this paper we are more interested in the regime of the ferromagnetic J'-bond, i.e., $J'/J < 0$ because the plaquettes are now frustrated. The quantum Monte Carlo method cannot be used for the frustrated system because of the sign problem. Instead, some mean-

field based approximation methods such as the renormalized spin wave theory (RSWT) [18], exact diagonalization [19] and coupled cluster method (CCM) [19] are used to study this regime. These studies found a phase transition at $J'/J = -1/3$ separating the Néel phase from a helical phase for classical spins, and the maximal frustration occurs around $J' \approx 1$ region. However, due the frustrations we suspect that a quantum spin liquid phase with topological order may appear around the region of maximal frustration. We indeed find this is the case from our study.

The paper is organized as follows. In the next section we describe the methods of the infinite time evolving block decimation(iTEBD) [26] and the the tensor-network renormalization group (TRG) [27, 28], which are used to solve the J-J' model, obtain the entanglement spectrum and topological entanglement entropy, and perform the quantum state renormalization. We also briefly review the above concepts. In section 3 we present the phase diagram of the J-J' model by evaluating the order parameter, entanglement entropy, dimer strength and the ground state energy. In section 4 we evaluate the topological entanglement entropy for the J-J' model and a toric code like state to characterize the topological phase. In section 5 we focus on various properties of the entanglement spectrum and its degeneracy to establish its connection with the topological order. Finally, we conclude our paper in section 6.

II. THE MODEL AND THE METHOD

The model we study in this paper is the staggered dimer model on square lattice, also known as the J-J' model. It is a quantum Heisenberg antiferromagnetic model with two kinds of nearest-neighbor exchange couplings, and its Hamiltonian is

$$H = J \sum_{<ij>} \vec{S}_i \cdot \vec{S}_j + J' \sum_{<ij>'} \vec{S}_i \cdot \vec{S}_j \ , \tag{1}$$

where the summations over $< ij >$ and $< ij >'$ represent sums over the nearest-neighbor bonds as shown in Fig.1. Each square lattice consists of three J bonds (the thin ones) and one J' bond (the thick one). We fix the J bonds to be antiferromagnetic, i.e., $J > 0$, and consider $-\infty < J'/J < \infty$ as the parameter of this model.

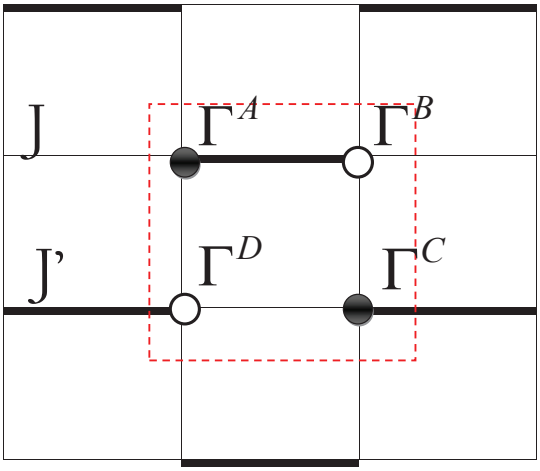

FIG. 1: The J-J' model on the 2D square lattice with two different nearest neighboring bond couplings J and J' (thin and thick, respectively). The red dash square is a 2×2 unit cell.

A. Solving the model with iTEBD and TRG

We will use the iTEBD algorithm [26] to find the translationally invariant ground state of the system in the form of the tensor product state ansatz

$$|\psi\rangle = \sum_{s_{1,1},s_{1,2},\ldots,s_{N,N}} tTr[A^{[1,1]}(s_{1,1})A^{[1,2]}(s_{1,2})\ldots A^{[N,N]}(s_{N,N})]|s_{1,1}, s_{1,2}, \ldots, s_{N,N}\rangle \qquad (2)$$

where $s_{i,j}$ labels the physical spin of dimension d_s at site (i,j) for $i,j = 1,\ldots,N$, $A^{[i,j]}_{r,d,l,u}(s_{i,j})$'s are rank-five tensors with the bond indices $r,d,l,u = 1,\cdots,\chi$, and tTr is to sum over all indices of tensors. We call χ the bond dimension and d_s the physical dimension. This ansatz captures the area law nature of the ground state's entanglement and yields a faithful representation for the ground states of many 2D spin systems.

The basic idea of iTEBD method is to evolve the system along the imaginary time in a very small time step so that the time evolution operator can be expanded as a sequence of two-site unitary operations through the Suzuki-Trotter decompositions. For long enough time evolution, the system will go to the ground state we are solving for. We further assume translational invariance of the ground state ansatz (2), then we only need to update 4 tensors as shown in Fig. 1 inside a unit cell for each time step.

Based on the solved ground state from iTEBD, we can calculate some quantities to char-

acterize the phase diagrams. For the symmetry breaking phase we can evaluate the order parameters which are the vacuum expectation value (vev) of some physical operators. However, when we insert a physical operator at some particular site such that the translational invariance is lost, one needs some efficient method to contract the exponentially large number of bounds. Here we will adopt the TRG method [27, 28] to do that. The basic idea of TRG is to renormalize the tensors of the TPS by keeping the relevant entanglement when coarse graining. In this way, we can reduce the size of the system while retaining the essential quantum correlations of the original ground state. Finally the whole system will be reduced to a unit cell with the renormalized tensor, we can then evaluate the vev's faithfully enough within the renormalized unit cell.

B. Order parameters for Néel and dimer phases

For the J-J' model considered here, we will evaluate the Néel order parameter i.e., given by $M_s^z = \frac{1}{M}\sum_{i=1}^{N}(-1)^i\langle\psi_g|S_i^z|\psi_g\rangle$ to characterize the Néel ordered phase. We also evaluate the spin-spin correlations and the dimerization [23–25]:

$$D_x = |\langle\vec{S}_{i,j}\cdot\vec{S}_{i+1,j}\rangle - \langle\vec{S}_{i+1,j}\cdot\vec{S}_{i+2,j}\rangle| \tag{3}$$

and

$$D_y = |\langle\vec{S}_{i,j}\cdot\vec{S}_{i+1,j}\rangle - \langle\vec{S}_{i,j}\cdot\vec{S}_{i,j+1}\rangle| \tag{4}$$

to characterize the dimmer strength of the disordered "dimer phase". Note that the Hamiltonian of the model does not possess the dimerized order by construction. Besides, we also use TRG to evaluate the ground-state energy per site as $\frac{E}{N} = \langle\psi_g|H|\psi_g\rangle/N$.

C. Characterizing topological phase by topological entanglement entropy

On the other hand, it is more difficult to characterize the topological phase since there is no symmetry breaking order parameter for it. On typical quantity for the 2D systems is the topological entanglement entropy [12, 13]. It is the sub-leading constant term in the entanglement entropy

$$S_L = \alpha L - \gamma + \mathcal{O}(L^{-\nu}) \,, \qquad \nu > 0 \,, \tag{5}$$

where L is the boundary size of the block for which the entanglement entropy is evaluated by tracing out the degrees of freedom outside it.

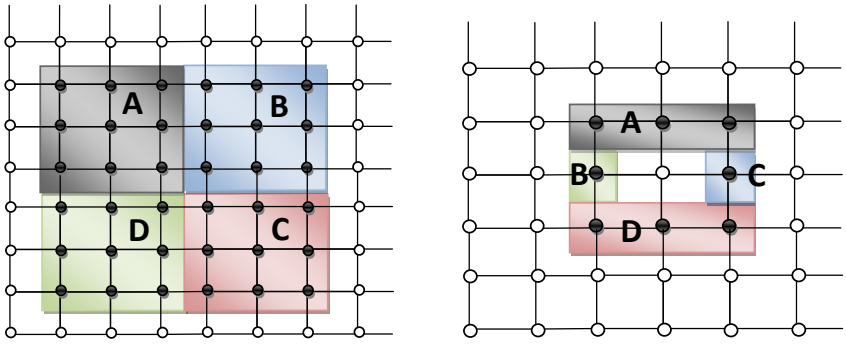

FIG. 2: Two schemes for evaluating the topological entanglement entropy. (Left) Kitaev-Preskill's scheme for the square block with even number of sites on each side. (Right) Levin-Wen's scheme for the square block with odd number of sites on each side.

Since the constant term γ is topological and universal, we can extract it by appropriately subtracting the entanglement entropies of different blocks. There are two subtraction schemes, one is proposed by Kitaev and Preskill [12], and the other is by Levin and Wen [13]. For the square lattice it is easier to implement the numerical evaluation of the entanglement entropy for a square or rectangular block. In this case, we find that it is convenient to adopt Kitaev-Preskill's scheme as shown in the left of Fig. 2 for the square block with even number of sites on each side of the square block. The extraction for the topological entanglement entropy then goes as follows

$$S_{topo}^{KP} = S_A + S_B + S_C + S_D - S_{AB} - S_{BC} - S_{CD} - S_{AD} + S_{ABCD} \ , \tag{6}$$

where $S_{AB..}$ denotes the von Neumann entropy of the density matrix $\rho_{AB...}$ in the region $AB... \equiv A \cup B \cup ....$

As for the square block with odd number of sites on each side, it is convenient to adopt Levin-Wen's scheme as shown in the right of Fig. 2, and the extraction is

$$S_{topo}^{LW} = S_{ABCD} - S_{ABD} - S_{ACD} + S_A + S_D \ . \tag{7}$$

In both cases, $S_{topo} = -\gamma < 0$, which is related to total quantum dimension D by $\gamma = LogD$ [12, 13].

D. Characterizing topological phase by degeneracy of entanglement spectrum

Another quantity in characterizing the topological phase is the degeneracy of the entanglement spectrum. It has been used to characterize the topological order for some quantum Hall states [14], and recently to characterize some symmetry-protected topological ordered Haldane phase in spin 1 chain [7]. In this paper, the entanglement spectrum is refereed to the spectrum of the Schmidt values for the bi-partition of the whole system. By definition, these Schmidt values are the eigenvalues of the reduced density matrix of either of the two partitions. Basically, the degeneracy of the entanglement spectrum implies the spins at different sites are almost in the maximally entangled state, hence it implies that the ground state has topological order. However, for general 2D spin system there is no consensus on the power of entanglement spectrum in characterizing the topological order, see [8] for recent study on this issue [1]. Despite that, one may expect that it still works in 2D since the topological order is closely related to the LRE characterized by the degeneracy of the entanglement spectrum.

Moreover, it is very easy and straightforward to evaluate entanglement spectrum for TPS by merging the tensors of neighboring sites and then doing singular value decomposition (SVD). This can be done by just using iTEBD without further invoking TRG. It is then easier than evaluating the order parameter, and definitely far more easier than evaluating the topological entanglement entropy.

Besides, from entanglement spectrum one can straightforwardly evaluate the bipartite entanglement measure per length as well as the single-site von Neumann entropy (1-tangle). Both can be used to characterize the quantum critical point [29].

[1] In [8], the entanglement spectrum of a bulk region is associated with a the boundary excitation spectrum. Their numerical study revealed that the boundary Hamiltonians become non-local for the topologically ordered states.

E. Quantum state renormalization

Since the topological order is closely related to the LRE, which however, is usually contaminated by the SRE. In order to make the characteristic of the topological order more explicit, one can implement the quantum state renormalization method [30–32], which can remove the short range entanglement by performing local unitary transformation. The successive quantum state renormalization will then flow the original state to a simpler fixed-point state, which, however, has the same topological order of the original state. We can then classify the topologically ordered phases by the TPS's tensors of the fixed-point states.

We now briefly describe the method as follows, and for more details see [31]. We first form a positive double tensor $\mathcal{T}$ by merging two layers of tensors T and $T^\dagger$ with the physical indices contracted. Note that the resultant double tensor is constructed so that it is invariant under the local unitary transformation, and then we can spectrally decompose it again back into two tensors $\tilde{T}$ with physical indices. The spectral weights encode the relevance of the entangled components. In this step we have removed the short range entanglement by the local unitary transformation taking the tensor T into $\tilde{T}$ according to the significance of the spectral weights. Next, we will coarse grain the lattice labelled by the tensor $\tilde{T}$ by implementing one step of block decimation in the TRG method.

After repeating the above steps the original TPS will then flow into a fixed-point state with all the SRE removed. If we perform quantum state renormalization while keeping the symmetry or gauge symmetry of the lattice, the final fixed-point tensors can then be used to classify the topological phases according to the symmetry structure.

III. NUMERICAL RESULTS FOR THE PHASE DIAGRAM OF J-J' MODEL

In this section, we will present the numerical results for the phase diagrams of the J-J' model of system size $N = 2^8 \times 2^8$.

We first evaluate the vev of staggered magnetization M_s^z in ground state as a function of J'/J by using the TRG method, and the result is shown in Fig. 2. In our calculation we consider the bond dimension up to $\chi = 5$ and keep $D_{cut} \geq \chi^2$ to ensure the accuracy of the TRG calculation. Here, D_{cut} is the cutoff on the bond dimension of the merging lattice during the coarse graining in the TRG method. We find that the numerical results converge

quickly already for $\chi = 4$ and the numerical program works efficiently. Therefore, we will take $\chi = 4$ and keep $D_{cut} = 24$ in our numerical study in this paper.

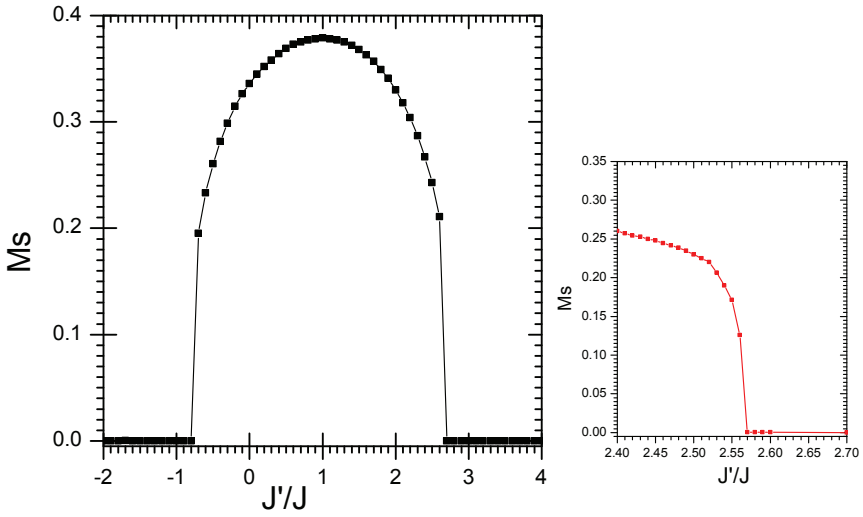

FIG. 3: Magnetization $\langle M_s^z \rangle$ v.s. J'/J (Magnified the regime around $J'/J \simeq 2.56$ in the right). The ground state is in the TPS ansatz with bond dimension $\chi = 4$ and $D_{cut} = 24$ for TRG in taking the vev. It indicates a second-order phase transition from Néel to a disordered (dimerized) phase at $J'/J \approx 2.56$, and another quantum critical point at $J'/J \approx -0.54$ separating the Néel phase from a possible topological phase.

From Fig. 3, it is observed that $\langle M_s^z \rangle$ drops to zero both at $J'/J \approx 2.56$ and $J'/J \approx -0.54$. This indicates two quantum critical points at the corresponding critical values of J'/J. It was known that a second-order transition from a Néel-ordered phase to a finite-gap disorder phase occurs at $J'/J \approx 2.51$, which is obtained from the unbiased quantum Monte Carlo simulation [21, 22]. Our result instead finds a critical point at $J'/J \approx 2.56$. The discrepancy could be due to the not large enough χ used in our numerical calculation. Furthermore, we fit the critical exponent β for the magnetization, i.e., $M_s = A|J' - J'_c|^\beta$. Our result is $\beta \simeq 0.37691$, which is close to the exponents of the 3D classical Heisenberg ($O(3)$) model, i.e., $\beta \simeq 0.3639 \pm 0.0035$ [2].

[2] By increasing χ one may improve the above the results to be close to the results by the quantum Monte Carlo method, though it may require far large computational power. In this work, we are more interested in the identification of the topological phase, and will be satisfied by the above accuracy for the $O(3)$ phase transition.

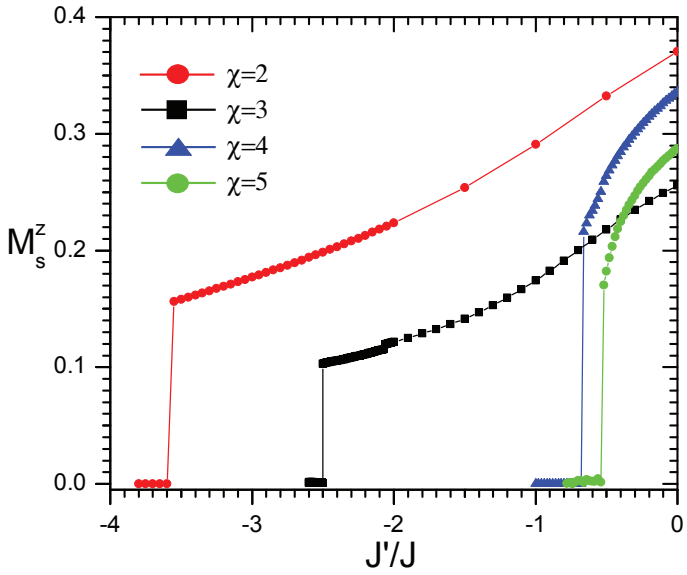

FIG. 4: $\langle M_s^z \rangle$ vs J'/J for different bond dimensions, the χ's. Larger χ yields a critical behavior more like a second order phase transition, other than the first order one. For $\chi = 5$ it indicates a second order phase transition at $J'/J \simeq -0.54$.

The other critical point at $J'/J \approx -0.54$ is frustrated since $J' < 0$ and $J > 0$, and there is possibility for the existence of topologically ordered phase due to the underlying degeneracy of the frustrated ground state. In Fig. 4 we show how the critical behavior in this regime changes when we change the bond dimension. Our result showing $\langle M_s^z \rangle = 0$ for $J'/J < -0.54$ is consistent with this expectation for a topologically ordered phase.

Since the system is frustrated in the regime of $J'/J < 0$, our method based on TPS and TRG will be more reliable than the others. Despite that, we still compare with the results from the other methods. It was shown that classically there is a second order phase transition from the Néel phase to a helical phase at $J'/J \simeq -1/3$ based on renormalized spin wave theory (RSWT) [18] or exact diagonalization (ED) [19]. Furthermore, it was claimed in [19] that the critical point shifts to $J'/J \simeq -1.35$ by using the coupled cluster method (CCM) to take the quantum fluctuations into account. However, we do not see such a shift in our results. Instead, we evaluate the ground state energy by TRG method and find the value is very close to the one obtained by the method of RSWT for a helical phase, especially in the Néel (classical) regime. The result is shown in Fig. 5. We see that for $J'/J < -0.5$ the agreement in energy between ours and RSTW's starts to deviate, and our translationally

invariant ground state is energetically more favored than the non-translationally invariant helical state. Similar deviation occurs for $J'/J > 2$, this again reflects the relevance of quantum effect when the system is away from the classical Néel ordered regime.

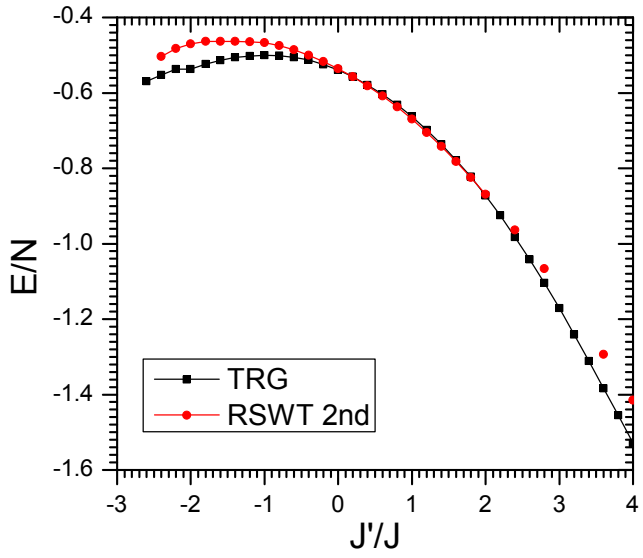

FIG. 5: Compare the ground state energy per site obtained from our TRG method and the RSWT.

For curiosity, we also calculate the dimerization D_x and D_y defined in (3) and (4) though they are not the order parameters of our dimerized model. The results is shown in Fig. 6. We see that $D_x = D_y = 0$ at $J'/J = 1$ as expected, otherwise they are nonzero and reach some constant values at the disordered (dimer) regime. To visualize the distribution of the dimer strength, in Fig. 7 we explicitly show the values of the spin-spin correlation of the neighboring sites for three different J'/J values.

Beside using the order parameter such as $\langle M_s^z \rangle$ in this case to characterize the quantum phase transitions, the entanglement measure can also do the job, see [29] for some examples. Especially, for the TPS ansatz it is quite straightforward to evaluate the bipartite entanglement per bond $S_{BP}^{\alpha} := -\sum_i \lambda_{\alpha,i}^2 \log \lambda_{\alpha,i}^2$, where $\alpha = J, J'$ labels the two different types of the bonds, and the $\lambda_{\alpha,i}$'s are the singular values obtained from the SVD of the site tensors in performing the iTEBD. Similarly, one can also use TRG to obtain the one-site reduced density matrix, and then evaluate the von Neumann entropy, i.e., 1-tangle denoted as S_1. The results are summarized in Fig. 8. Note that the derivatives of both S_1 and $S_{BP}^{J,J'}$ are discontinuous at two quantum critical points. Moreover, it shows that the classical Néel

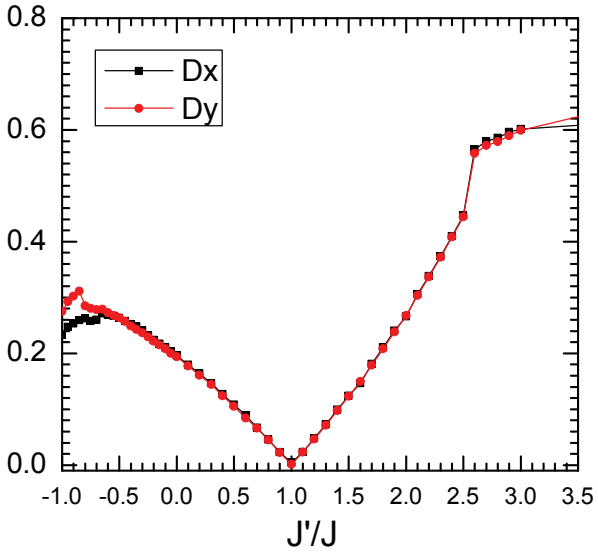

FIG. 6: Dimerization D_x and D_y vs. J'/J.

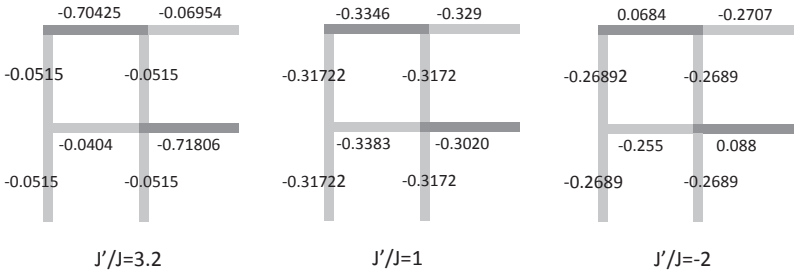

FIG. 7: Visualization of Spin-Spin correlation of neighboring sites for $J'/J = 3.2$ (disordered dimer phase), $J'/J = 1$ (Néel phase) and $J'/J = -2$(possibly topologically ordered phase).

regime has lower entanglement compared to the other two phases dictated by the significant quantum effect. For the disordered dimer phase with $J'/J > 2.56$ quite amount of the quantum entanglement is due to the formation of the dimers, i.e., nearest-neighboring sites form the maximally entangled states (Bell states). Once the dimer is formed, the sites on the both ends of the dimer will not be correlated with the other sites, i.e., the monogamy of the entanglement.

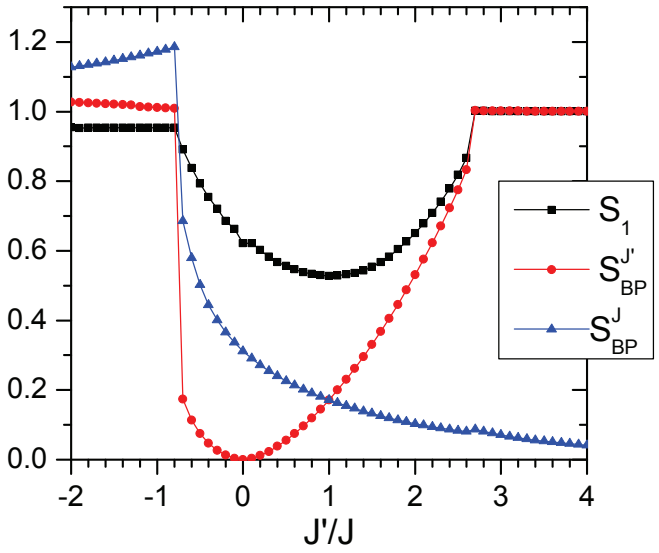

FIG. 8: The entanglement measures $S_{BP}^{J,J'}$ and S_1 v.s. J'/J. The discontinuities in the derivative of the entanglement measure occur right at the quantum critical points, and the classical Néel regime has lower entanglement.

The local nature of SRE for the dimer phase is different from the LRE for the topological phase in the regime $J'/J < -0.54$. Later, we will see that the difference between these twos will be reflected in the degeneracy of the entanglement spectrum.

IV. TOPOLOGICAL ENTANGLEMENT ENTROPY

In this section, we will evaluate the topological entanglement entropy based on TPS ansatz. We will consider first the J-J' model, and then a toric code like toy TPS state to demonstrate the power of TRG method in identifying the topological phase.

A. J-J' model

In order to make sure that the phase in the regime $J'/J < -0.54$ is the topological phase, we evaluate the topological entanglement entropy (i.e., $-\gamma$) according to the prescriptions mentioned before. We also find that the entanglement entropy increases linearly with the block boundary size, this gives a consistent check for our numerical codes.

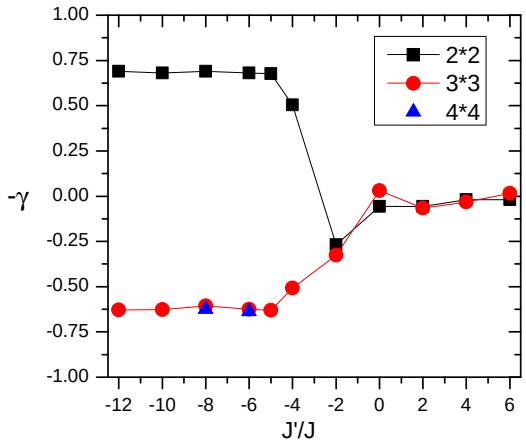

FIG. 9: Topological entanglement entropy vs. J'/J for the 2 by 2 block (square), the 3 by 3 block (circle) and the 4 by 4 block (triangle) for J-J' model.

Our result is shown in Fig. 9. The one for 2 by 2 block is evaluated by Kitaev-Preskill's scheme, and the one for 3 by 3 block by Levin-Wen's scheme. For larger blocks, it requires far more power of computation in TRG for evaluating the block entanglement entropy. For example, if we would like to evaluate the entanglement entropy for the 4 by 4 block, then the number of entries for the reduced density matrix will be about $2^{16}/2^9 = 128$ times of the one for 3 by 3 block. That means it will take about 100 times of the computing time than for the 3 by 3 block, and it is beyond our computational capacity. This is the disadvantage when trying to identify the topological phase with the topological entanglement entropy numerically. Despite that, we still spent months to evaluate the topological entanglement entropy for the 4 by 4 block at $J'/J = -6, -8$ as shown in Fig. 9. The values of these two data points are quite consistent with the ones for the 3 by 3 block. More closely, for the 3 by 3 block $\gamma = 0.6248$ at $J'/J = -6$ and $\gamma = 0.6057$ at $J'/J = -6$, and for the 4 by 4 block $\gamma = 0.6276$ at $J'/J = -6$ and $\gamma = 0.6111$ at $J'/J = -6$, respectively.

Our result shows that γ is consistent with zero for the non-topological phases (Néel and dimer phases). However, we find that γ is negative and unphysical in the topological phase for 2 by 2 block. This could be due to the small boundary size effect from the next sub-leading term of $\mathcal{O}(L^{-\nu})$ with $\nu > 0$. On the other hand, for the 3 by 3 block we expect the small boundary size effect could be suppressed so that γ in the topological phase should be positive. We find that this is indeed the case, and this is also confirmed by the two data

points for the 4 by 4 block. In Fig. 9, there is a long crossover for γ as we vary J'/J between 0 and -5. Then, γ approaches 0.6 around $J'/J = -5$ and then remains at that value for more negative J'/J as expected from its topological nature. Naively, we expect a quantum critical point separating topological and non-topological phase, and the crossover could be due to the SRE in our TPS solution. We expect that it should be removed by suitable quantum state renormalization.

Though our result is subjected to the errors from the small size effect and also from the approximation in our numerical method of iTEBD and TRG, it does indicate a nonzero γ and thus a topological phase in the regime with $J'/J < -0.54$. We may expect the value of γ will be improved if the above errors could be reduced.

B. Toric code like state

Due to the limitation of our computation power, it is hard to evaluate the topological entanglement entropy to high precision by increasing the bond dimension χ in the TPS ansatz for the J-J' model. Instead, we now consider a toric code like TPS state proposed in [31] with $\chi = 2$. In this case we can evaluate the topological entanglement entropy more precisely to characterize the topological order, and demonstrate the power of TRG method on this issue. Later on, we will compare the topological entanglement entropy of this state with the pattern of degenerate entanglement spectrum of the same state, and demonstrate that the latter can be also used to characterize the topological order without invoking heavy computation capacity.

This toy TPS state on the square lattice motivated by the toric code model is characterized by the TPS tensor on each vertex in Fig. 10 in the form of $T^{ijkl}_{\alpha\beta\gamma\delta}$ with four physical indices $i, j, k, l = 0, 1$ and four bond indices $\alpha, \beta, \gamma, \delta = 0, 1$ (i.e., bond dimension $\chi = 2$). Its entries are given by

$$T^{ijkl}_{ijkl} = \begin{cases} g^{i+j+k+l} \ , \ \text{if} \quad i+j+k+l = 0 \mod 2 \ , \\ 0 \ , \qquad\qquad\qquad\qquad \text{otherwise.} \end{cases} \tag{8}$$

For $g = 1$, it reduces to the ground state of the toric code model with $\mathbb{Z}_2$ topological order. For $g = 0$, it reduces to a trivial product state. Therefore, as we vary g, the state will go through a phase transition, and in [31] it showed that the quantum critical point occurs at $g_c \simeq 0.8$ which separates the $\mathbb{Z}_2$ topological phase from the phase of product state.

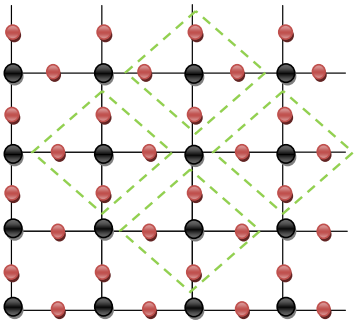

FIG. 10: The toric code is defined on a 2D square lattice. The red dot is a spin 1/2 particle located on each link. After splitting every spin 1/2 into two, each vertex (black dot) on the lattice lives a TPS tensor with four physical indices, and four bond indices. The (green) dashed line square is a 2 by 2 block for which we evaluate the topological entanglement entropy for the toric code like TPS state.

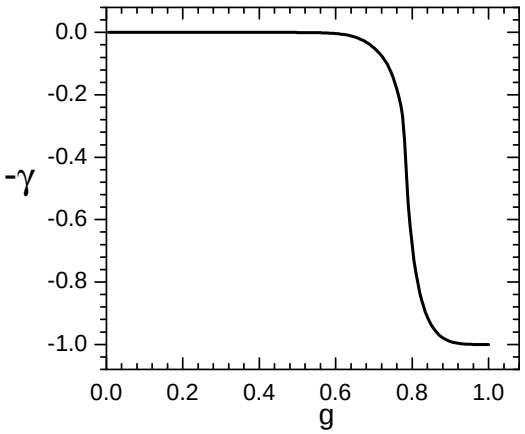

FIG. 11: Topological entanglement entropy from Kitaev-Preskill's scheme for the 2 by 2 block in Fig. 10.

With the above TPS state, we then use the Kitaev-Preskill's scheme to numerically evaluate the topological entanglement entropy for 2 by 2 block indicated by the blue dash line in Fig. 10. Since this state has only $\chi = 2$ and thus requires not much computation power to carry out the numerical calculation up to high precision. Again, we verify that the

entanglement entropy obeys the area law. Our result is shown in Fig. 11, and it indicates a crossover around $g_c \simeq 0.8$ separating the trivial phase with $\gamma = 0$ and the topological phase with $\gamma = 1$. We may observe a sharp jump at g_c if we increase the block size, however, it is then beyond our computation capacity.

V. DEGENERACY OF ENTANGLEMENT SPECTRUM AND TOPOLOGICAL ORDER

In general, there are some ways of classifying the possible topological phases, however, there is no specific method with consensus in identifying the topological phase of a particular dynamical model. Topological entanglement entropy [12, 13] is usually thought to be good index in characterizing the topological order, but it is difficult to evaluate numerically to high precision due to the limitation of the computation capacity as discussed in the previous section.

On the other hand, the degeneracy of the entanglement spectrum has recently implemented to characterize the topological orders for some 2D quantum Hall states [14] and some 1D symmetry protected topological phase [7]. Despite there is no rigorous proof on its power of characterizing the 2D topological orders, the degeneracy of the entanglement spectrum by itself indicates the existence of the LRE. Recently it is argued that the LRE is the characteristics of the topological order from the point of view of the quantum information [3–5, 7]. The tensor of the TPS encodes the information about the entanglement for the bi-partitions of the system. The entanglement spectrum obtained from it weighs different components of quantum correlation between bi-partition regions in the ground state wave function. Therefore, if there is a double degeneracy of the entanglement spectrum, it means that the bi-partitions are almost in the maximally entangled states. It is the LRE since it involves the the collective coherences of the spins on half of the space to be strongly correlated with all the spins in the other half.

A. Some examples

Instead of providing the proof of the above picture, we give examples. A well-studied one is the symmetry-protected Haldane phase, which is described by the Afflect-Kennedy-Lieb-

Tasaki (AKLT) state. The AKLT state can be put into the form of the MPS represented by the matrices $\{A_i\} = \{\sigma^z, \sqrt{2}\sigma^+, -\sqrt{2}\sigma^-\}$. By merging two matrices and then performing SVD, we find that the singular values, i.e., the entanglement spectrum, are doubly degenerate. This is also proved in more rigorous way in [7]. Since the topological phase is robust again small perturbations, we can consider the deformed AKLT Hamiltonian

$$H = J \sum_i \vec{S}_i \cdot \vec{S}_{i+1} + U_{zz}(S_i^z)^2 \ . \tag{9}$$

At the large U_{zz}, there is a trivial phase where all the spins are in the eigenstates of S^z . We use the iTEBD method to solve the ground states in the MPS ansatz and then find the entanglement spectrum. We find that the phase transition between Haldane phase and the trivial phase is characterized by the degeneracy of the entanglement spectrum.

The relation between the degeneracy of the entanglement spectrum and the topological order for the 2D spin system is less explored. Here we consider the simplest $\mathbb{Z}_2$ toric code model [10], and the explicit TPS form of its ground state is represented by the tensor $T^{ijkl}_{\alpha\beta\gamma\delta,\mathbb{Z}_2}$ as discussed in the previous section. We can find the entanglement spectrum by merging the tensors and then performing SVD. Again, we find it is 2-fold degenerate.

B. Topological order of J-J' model by entanglement spectrum and its robustness

The entanglement spectrum for each bond in the J-J' model from the TPS of our numerical ground state solution is given in Fig. 12(a). Each small circle with a middle bar represents a specific singular value of the entanglement spectrum. Note that both J- and J'-bond show the similar degeneracy pattern, so in the following we only show one of them. We see that the singular values are doubly degenerate for the regime $J'/J > -0.54$ in which the Néel order also vanishes. Therefore, $J'/J = -0.54$ should be the critical point separating the topological and non-topological phases, along with the evidence of nonzero topological entanglement entropy discussed previously.

Recall that the precision for the topological entanglement entropy and the sharp quantum transition point is hard to achieve due to the limitation on the computation capacity. However, with the same capacity we can obtain the degenerate entanglement spectrum quite easily with a sharp quantum transition point. In contrast with the topological entanglement entropy, this is the advantage to use the degenerate entanglement spectrum to characterize

the topological order numerically with TPS ansatz.

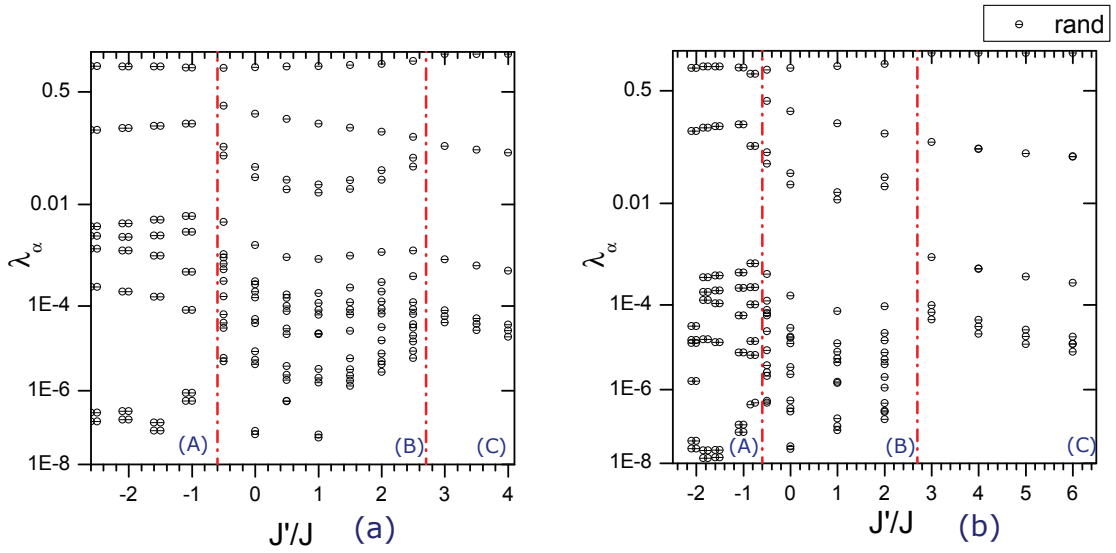

FIG. 12: (a) Entanglement spectrum per bond of the J-J' model. (b) Entanglement spectrum of the J-J' model with the random perturbation.

Since the topological order should be robust against the local perturbations, the degeneracy of the entanglement spectrum should also does so if it can be used to characterize the topological orders. We first add a random perturbation H_{rand} at each step of iTEBD, where the random 2-body Hamiltonian H_{rand} is a real symmetric matrix with 10 independent matrix elements given by the random numbers in the interval $[0, 0.1J]$. The result is shown in Fig. 12(b). We see that the entanglement spectrum is changed but the pattern of its degeneracy remains intact. This demonstrates the robustness of the degeneracy of the entanglement spectrum, and thus the robustness of the topological order.

To further check the robustness, we add a perturbation of the form $h\sum_{i,j} S^z_{i,j}$ which breaks the spin SO(3) symmetry and the time-reversal symmetry. For small h, the above perturbation does not destroy the double degeneracy of the entanglement spectrum. Once h is larger than the critical value 1.2, the double degeneracy will be lost. The results for $h = 0.1$ and $h = 1.2$ are shown in Fig. 13(a) and (b), respectively. On the other hand, in Fig. 13(c) we show the result by adding a perturbation of the form $t\sum_{i,j}(-1)^j \vec{S}_{i,j} \cdot \vec{S}_{i,j+1}$ which breaks the translational symmetry in the direction perpendicular to the dimers. Again, we see that the perturbation with $t = 0.1$ cannot destroy the double degeneracy.

With above generic types of perturbation, we see that the degeneracy pattern of the

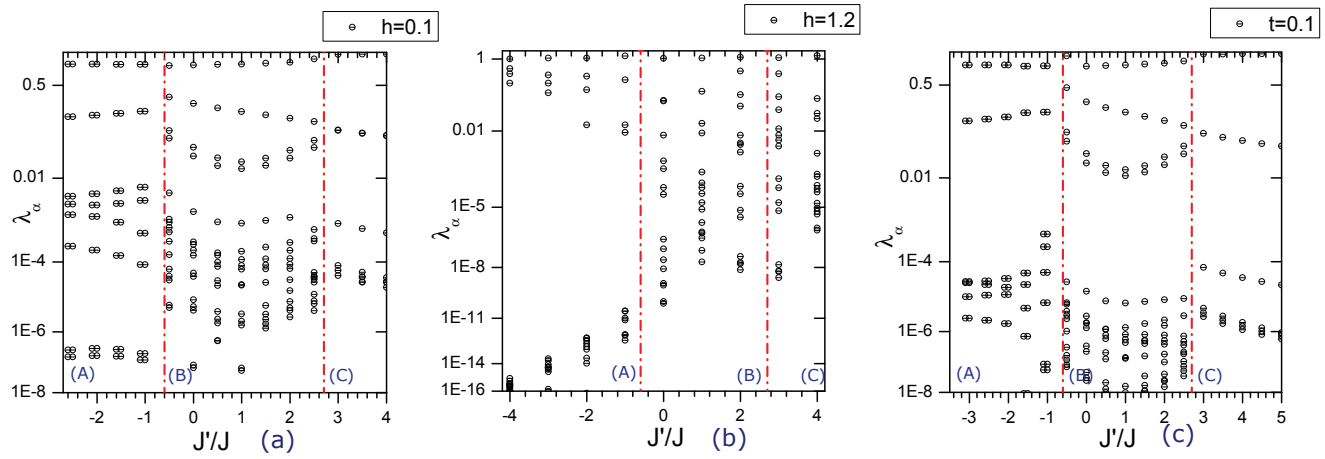

FIG. 13: Entanglement spectrum per bond of the J-J' model perturbed by $h\sum_{i,j} S^z_{i,j}$ with (a) $h = 0.1$, (b) h=1.2 (critical value), and (c) perturbed by $t\sum_{i,j}(-1)^j \vec{S}_{i,j} \cdot \vec{S}_{i,j+1}$ with $t = 0.1$. The degeneracy pattern of the entanglement spectrum is robust under the symmetry-breaking perturbations.

entanglement is quite robust, this reflects the topological nature of the phase.

C. Remove short range entanglement

As described previously, quantum state renormalization consists of two steps: the first step is to optimize the local unitary transformation to remove the SRE, and the second step is to coarse grain the site tensors according to the TRG like method while keeping the physical bonds. After successive steps of quantum state renormalization, the TPS will flow to a fixed point with most of SRE being removed. Therefore, one would expect the fixed-point TPS will be the representative of the universal class of topologically ordered states. This quantum informational way of classifying the topological orders are recently proposed in [3–5, 7, 31].

We then would like to study how the entanglement spectrum evolves under the quantum state renormalization group (RG) flow procedure. Since we conjecture that the degeneracy pattern of the entanglement spectrum encodes the LRE, we would expect it is robust under the quantum state renormalization, which only removes the SRE. This is indeed the case for the J-J' model and the result is shown in Fig. 14. Moreover, we see that under the quantum state RG flow, the number of the dominant singular values decreases in the topological

phase. We can think of the extreme case that there is only one dominant doubly degenerate singular value with all others being suppressed, then the whole lattice is in the GHZ state, i.e., maximal LRE. So, the suppression of the singular values except the dominant ones corresponds to the removal of the SRE under the quantum state RG flow, and the LRE will be encoded in the degeneracy of the dominant singular values of the fixed-point TPS.

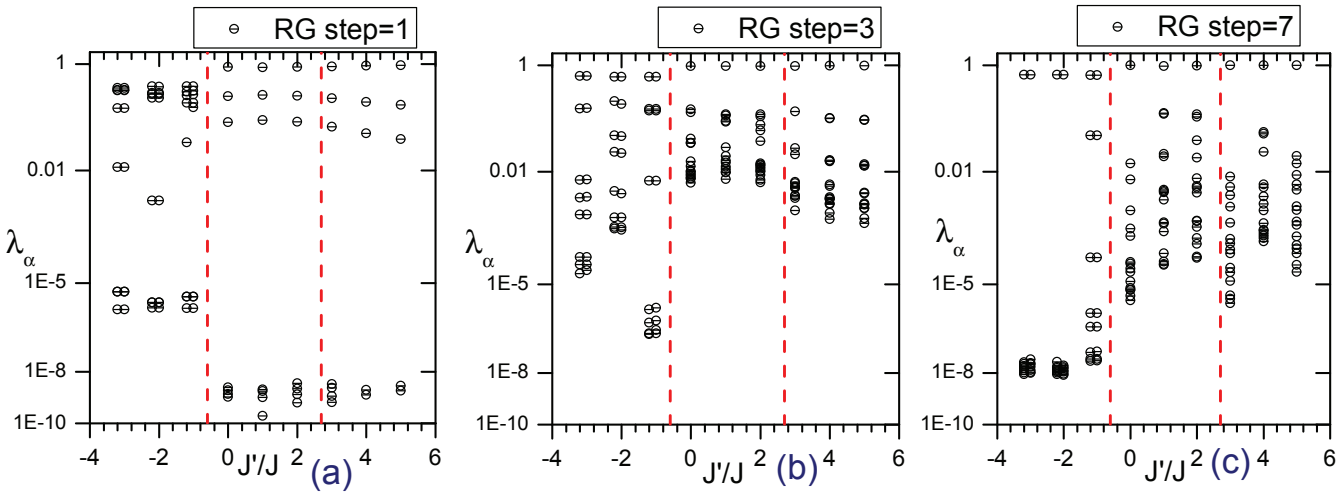

FIG. 14: The entanglement spectrum of J-J' model under quantum state RG flow. The number of the RG steps is labelled accordingly.

Finally, to understand more about the entanglement spectrum under quantum state RG flow, we consider the case for the toric code like TPS state (8) discussed before. To draw a parallel comparison with the topological entanglement entropy presented in Fig. 11, we evaluate the difference between the two largest singular values of the entanglement spectrum, denoted as $|\lambda_1 - \lambda_2|$. The result is shown in Fig. 15.

From Fig. 15, we see that before quantum state renormalization, it seems there is no degenerate entanglement spectrum except at $g = 1$. Moreover, the degeneracy at $g = 1$ is 2-fold, which may reflect the underlying $\mathbb{Z}_2$ symmetry apart from the LRE. This is in sharp contrast to the crossover behavior of topological entanglement entropy around $g \simeq 0.8$ as shown in Fig. 11. However, after one step of quantum state renormalization, we obtain the crossover similar to the one for topological entanglement entropy. As we perform more steps of quantum state renormalization, the crossover become sharper and sharper around $g_c = 0.8$. It finally approaches to a sharp quantum critical point separating the topological phase ($g > g_c$) from the non-topological one ($g < g_c$). Similar behavior for some scale

invariant quantity of the same state (8) under quantum state RG flow is also found in [31].

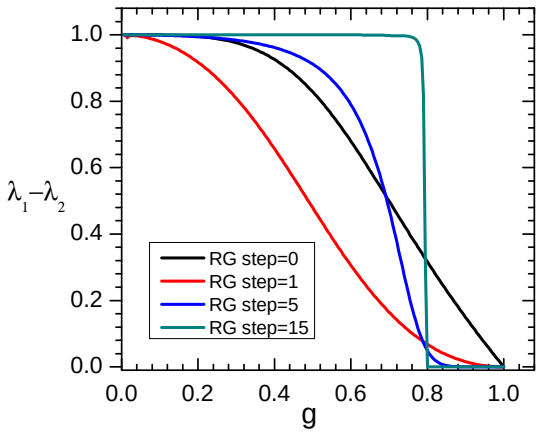

FIG. 15: The difference between the two largest singular values of toric code like model as a function of g under the renormalization flow.

Moreover, we can get some lesson as follows. Though the degeneracy of the entanglement spectrum indicates the existence of the LRE, the reverse statement may not be true due to the contamination of the SRE. However, the hidden LRE and the underlying symmetry such as $\mathbb{Z}_2$ for the toric code ground state will emerge under the quantum state RG flow as shown in Fig. 15.

VI. CONCLUSION

In this paper, we identify a new topological phase for the J-J' model by explicitly calculating the phase diagram of order parameters, topological entanglement entropy and the degeneracy of the entanglement spectrum. This result demonstrates that the recent quantum information inspired methods such as TPS, iTEBD and TRG are powerful enough in tackling the frustrated spin systems and identifying the topological orders. Especially, we demonstrate that the concepts of SRE and LRE introduced in [3, 4] are very useful in providing intuitive picture for the entangled nature of topological order. It is also helpful in interpreting the numerical results based on TPS ansatz.

We have also found an intriguing connection between the degeneracy of the entanglement spectrum and topological order by explicitly solving the J-J's model as a nontrivial example. The topological order may not always reflect in the degeneracy of the entanglement spectrum due to the disturbing SRE. However, as we show explicitly, we can remove SRE by quantum state renormalization so that the degeneracy of the entanglement spectrum after quantum state renormalization indicates the topological order. The implication of such a connection is far-reaching in numerical identification of the topological phase in 2D systems since the computation power of obtaining the entanglement spectrum is far less than the one of evaluating the topological entanglement entropy.

Based on our observation, we believe that we can use the degeneracy of the entanglement spectrum based on TPS ansatz to identify the topological phases of other interesting frustrated 2D systems. We will report more works along this direction in the near future.

Acknowledgements

We thank H.Y. Chen, Z. C. Gu and A. Sandvik for helpful discussions. We also thank Yu-Cheng Lin for the generous support on computer facility. This work is also supported by Taiwan's NSC grant 97-2112-M-003-003-MY3. We also thank the support of NCTS.

---

[1] T. Senthil, A. Vishwanath, L. Balents, S. Sachdev and M. P. A. Fisher, Science 303, 1490 (2004).

[2] T. J. Osborne and M. A. Nielsen, Phys. Rev. A 66, 032110 (2002).

[3] Z.-C. Gu and X.-G. Wen, Phys. Rev. B **80**, 155131 (2009); X. Chen, Z.-C. Gu, and X.-G. Wen, arXiv:1008.3745 and arXiv:1103.3323.

[4] X. Chen, B. Zeng, Z.-C. Gu, I. L. Chuang, and X.-G. Wen, Phys. Rev. B **82**, 165119 (2010); Z.-C. Gu, Z. Wang, and X.-G. Wen, arXiv:1010.1517.

[5] N. Schuch, D. Pérez-García, and I. Cirac, arXiv:1010.3732.

[6] F. Pollmann, E. Berg, A. M. Turner, and M. Oshikawa, arXiv:0909.4059.

[7] F. Pollmann, E. Berg, A. M. Turner, and M. Oshikawa, Phys. Rev. B **81**, 064439 (2010).

[8] J. I. Cirac, D. Poilblanc, N. Schuch, F. Verstraete, arXiv:1103.3427.

[9] F. Verstraete, J. I. Cirac, arXiv:cond-mat/0407066; V. Murg, F. Verstraete, and J. I. Cirac, Phys. Rev. A. 75, 033605(2007).

[10] A. Yu. Kitaev, Ann. Phys. (N.Y.) **303**, 2 (2003).

[11] S. Dusuel, M. Kamfor, R. Orus, K. P. Schmidt, J. Vidal, Phys. Rev. Lett. **106**, 107203 (2011).

[12] A. Kitaev and J. Preskill, Phys. Rev. Lett. **96**, 110404 (2006).

[13] M. Levin and X.-G. Wen, Phys. Rev. Lett. **96**, 110405 (2006).

[14] H. Li and F. D. M. Haldane, Phys. Rev. Lett. **101**, 010504 (2008).

[15] X. G. Wen and Q. Niu. Phys. Rev. B. **41**, 9377 (1990).

[16] B. A. Friedman and G. C. Levine. Phys. Rev. B **78**,035320 (2008).

[17] R. R. P. Singh, M. P. Gelfand, and D. A. Huse, Phys. Rev. Lett. **61**, 2484 (1988).

[18] N.B. Ivanov, S.E. Krüger, and J. Richter, Phys. Rev. B **53**, 2633 (1996).

[19] S.E. Krüger, J. Richter, D. J. J. Farnell and R. F. Bishop, Phys. Rev. B **61**, 14607 (2000).

[20] B. Bauer, G. Vidal, M. Troyer, J. Stat. Mech. P09006 (2009).

[21] S. Wenzel, L. Bogacz, and W. Janke1, Phys. Rev. Lett. **101**, 127202 (2008).

[22] F.-J. Jiang, arXiv:0911.0653.

[23] P. W. Leung and N.-w. Lam, Phys. Rev. B **53**, 2213 (1996).

[24] R. R. P. Singh, Z. Weihong, C. J. Hamer,and J. Oitmaa, Phys. Rev. B **60**, 7278 (1999).

[25] Yongmin Yu and G. Müller, V. S. Viswanath, Phys. Rev. B **54**, 9242 (1996).

[26] G. Vidal, Phys. Rev. Lett. **98**, 070201(2007); R. Orús and G. Vidal, Phys. Rev. B. **78**, 155117 (2008).

[27] M. Levin and C. P. Nave, Phys. Rev. Lett. **99**, 120601 (2007).

[28] Z. C. Gu, M. Levin and X. G. Wen, Phys. Rev. B. **78**, 205116 (2008).

[29] C. Y. Huang and F. L. Lin, Phys. Rev. A **81**, 032304 (2010).

[30] R. Orús, Phys. Rev. Lett. **100**, 130502 (2008).

[31] X. Chen, Z.-C. Gu, and X.-G. Wen, Phys. Rev. B. **82**, 155138 (2010).

[32] F. Verstraete, J. I. Cirac, J. I. Latorre, E. Rico, and M. M. Wolf, Phys. Rev. Lett. **94**, 140601 (2005).